Broadband leaky Lamb waves excited by optical breakdown in water

Citation: Athanassiadisa, Athanasios G. and Douglas P. Hart. "Broadband leaky Lamb waves excited by optical breakdown in water." Journal of the Acoustical Society of America 146, 2 (August 2019): 885–892 © 2019 Acoustical Society of America

As Published: http://dx.doi.org/10.1121/1.5120182

Publisher: Acoustical Society of America (ASA)

Persistent URL: https://hdl.handle.net/1721.1/123821

Version: Final published version: final published article, as it appeared in a journal, conference proceedings, or other formally published context

Broadband leaky Lamb waves excited by optical breakdown in water

Athanasios G. Athanassiadis[a] and Douglas P. Hart
Department of Mechanical Engineering, Massachusetts Institute of Technology, 77 Massachusetts Avenue, Cambridge, Massachusetts 02139, USA

(Received 21 March 2019; revised 31 May 2019; accepted 12 July 2019; published online 1 August 2019)

Optical breakdown of water is used as a sound source to excite a broadband set of leaky Lamb waves in submerged aluminum plates. The source is shown to simultaneously excite guided modes spanning 0.1–5 MHz in frequency and 0–0.8 mm^{-1} in wavenumber. The measured response overlaps well with dispersion curves for Lamb waves in the plates, revealing strong coupling to both symmetric and antisymmetric modes. The strongest responses arise when a mode's phase velocity approximately equals the plate's compressional wave velocity. These results are shown to arise from an interplay of the sensing geometry, guided wave speeds, and signal processing. Finally, implications for non-contact sensing are discussed. © *2019 Acoustical Society of America.*
https://doi.org/10.1121/1.5120182

[MRH] Pages: 885–892

I. INTRODUCTION

When an elastic plate is excited by a high-frequency sound source, guided Lamb waves can develop and travel along the plate.[1] Such waves are used extensively to characterize materials and structures across scientific and industrial applications. For instance, Lamb waves can be used to measure sound speed, gauge thickness, and identify defects in a metal plate or structure.[2–5] If the plate is submerged in water, then some of the plateborne Lamb waves will couple to the fluid and radiate acoustic plane waves into the water.[1,2,6] These leaky Lamb modes can be used to remotely measure a structure's response, providing a mechanism for completely non-contact structural evaluation.[7–9]

However, the coupling between elastic guided waves and acoustic waves in the fluid can make it challenging to remotely measure the properties of submerged structures. In general, a Lamb wave at frequency f and modal wavenumber $k_m(f)$ can only couple to acoustic waves in the water if the mode's phase velocity exceeds the sound speed in water, i.e., $v_m = f/k_m > c_w$.[1,2] For such modes, the waterborne acoustic waves propagate at a mode-dependent critical angle $\theta_{c,m}$ from the plate, defined by the coincidence-matching condition: $\cos\theta_{c,m} = c_w/v_m(f)$. In order to excite and receive the guided wave response using transducers in the water, the transducer frequency must match the mode of interest and the transducers must be oriented at the (f and k_m-dependent) critical angle. In practice, this imposes strict alignment constraints ($<1^\circ$ tolerance) for measurements with a narrow-band, directional underwater transducer.[7,8] Additionally, such measurements only couple to structural information at one frequency and k_m at a time. To evaluate a plate's properties at a different f and k_m would thus require different transducers and realignment of the sensing system. Such methods quickly become infeasible for measurements of real structures, where a broadband response is desirable to identify defects or mechanical features across multiple length scales or uncertain materials.

A wider-band Lamb wave response can be remotely excited using laser absorption at the plate's surface and measured by a broadband hydrophone in the water. But to date, such remote laser techniques have only been used to measure a narrow-band response from low-order Lamb modes.[9] Furthermore, such laser excitations are sensitive to the plate's optical properties, so the technique may not be applicable for transparent, fouled, or occluded inspection targets. If a more flexible acoustic source could excite broadband leaky Lamb waves in underwater plates, then it would enable more versatile non-contact guided wave measurements in challenging environments where contact is not possible.

Recently, optical breakdown has emerged as a unique source of underwater sound. Optical breakdown is a nonlinear optical process that occurs when a high-power laser pulse is focused tightly into the water, ionizing a plasma. The plasma absorbs energy from the laser pulse and then expands explosively, radiating a strong, broadband acoustic shock.[10] Because the breakdown plasma is very localized (sub-millimeter scale), the acoustic source is point-like, and the initial shock wave decays into a linear acoustic wave after a few millimeters of propagation[11,12] Therefore, by focusing a high-power laser into water, it is possible to remotely create a loud, impulsive acoustic point source.

These characteristics make optical breakdown a valuable acoustic source that can overcome existing challenges in underwater measurements. Because the source is created optically, it shares spatial flexibility with traditional laser acoustic sources. And because of the nonlinear optical processes involved, breakdown generates a louder, more broadband signal than comparable linear laser techniques.[13] Additionally, by driving breakdown in the water, the acoustic source is decoupled from the target, and could thus insonify a wider range of materials, regardless of their surface

[a]Electronic mail: thanasi@alum.mit.edu

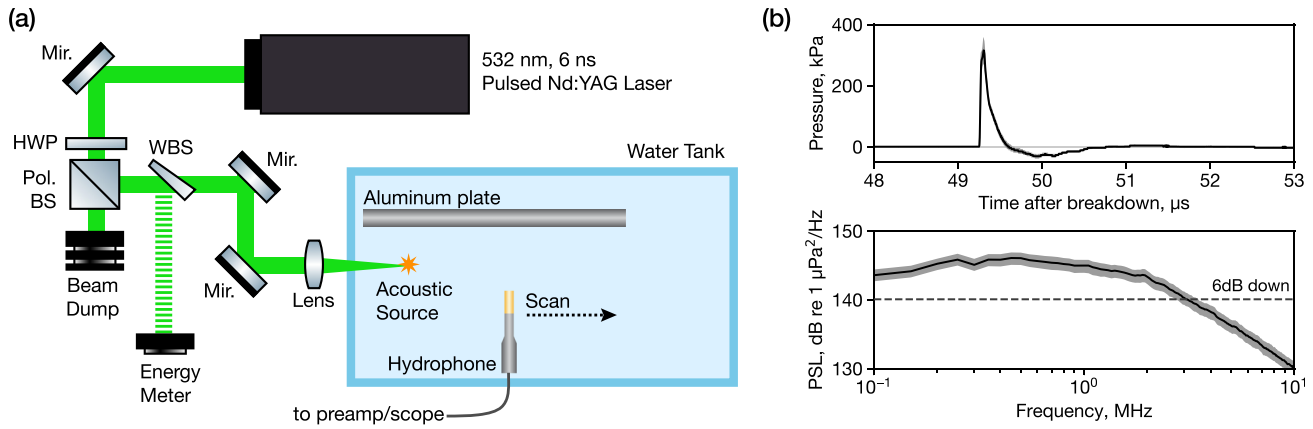

FIG. 1. (Color online) Experimental setup and acoustic source characteristics. (a) Aluminum plates were submerged in the aquarium, insonified by an optical breakdown acoustic source, and the response was recorded by a hydrophone, which was scanned to simulate an array. To generate the acoustic source, a high power laser was attenuated by a half waveplate (HWP) and polarizing beam splitter (Pol. BS), then redirected to a focusing lens using high-power mirrors (Mir.). Within the optical path, a wedge beam sampler (WBS) and energy meter were used to monitor the laser energy each pulse. Optical breakdown occurred at the focus of the lens, and consistently produced a broadband source. (b) Source pressure signal, measured directly in front of the source at 7.5 cm range, with hydrophone perpendicular to the laser axis. The pressure rises rapidly to a peak and then decays exponentially with a small negative phase. The power spectrum level reveals a broadband source with a 6 dB bandwidth larger than 3 MHz. The solid black lines represent the median of 1000 measurements, and the shaded error bars span between the 20th and 80th percentiles of the data.

optical properties. Finally, because the source radiates omnidirectionally, it circumvents the tight coincidence-matching constraints of traditional immersion transducers.

Despite these useful characteristics, optical breakdown has not been widely investigated as a high-frequency underwater sensing source. Therefore, it remains to be seen how effectively the source can couple to a useful response from underwater structures.

In this article, we demonstrate that leaky Lamb waves can be excited in aluminum plates by a waterborne optical breakdown source. With the single source, it is possible to remotely excite Lamb modes across a broadband window of frequencies and wavenumbers. Although the leaky response is significantly weaker than the excitation signal, we demonstrate how it can be isolated in the time domain by leveraging the flexibility in the source positioning and a simple ray model. This signal isolation allows the dispersive structure of the guided modes to be clearly identified in the frequency domain. The measured dispersive response is shown to overlap well with theoretical dispersion curves for plates of three different thicknesses. Finally, we discuss the structure of the frequency domain response and its implications for noncontact guided wave sensing.

II. MATERIALS AND METHODS

A. Experimental methods

As shown in Fig. 1, acoustic measurements were made in a $0.9\,\mathrm{m} \times 0.3\,\mathrm{m} \times 0.3\,\mathrm{m}$ tank filled with water (5 μm particle-filtered and deionized). An aluminum plate was submerged in the water, insonified by the optical breakdown acoustic source, and the response was recorded with a high-frequency hydrophone. To simulate an array response, the hydrophone was scanned parallel to the plate and experiments were repeated for each hydrophone position.

Three plates were tested, all composed of 6061 aluminum, with 30.5 cm length and 15.2 cm height. The three plates had different thicknesses ($d = 3.12$, 6.45, and 9.65 mm) in order to measure different guided wave responses. To compare the measurements to theory, dispersion curves were calculated for the plates by numerically solving the Rayleigh–Lamb equation for an unloaded plate.[2] For these calculations, the known plate thicknesses were used along with typical values of the longitudinal and transverse wave speeds in aluminum ($c_L = 6.32$ mm/μs and $c_T = 3.13$ mm/μs, respectively).[14] The phase and group velocity dispersion curves are plotted in Fig. 2 for the first four symmetric and antisymmetric modes.

Sound was produced by focusing a Q-switched Nd:YAG laser (Quantel Brilliant B) into the tank, causing the water to undergo optical breakdown. The laser pulse duration was 6 ns, the wavelength was 532 nm, and the beam diameter was 8 mm. The laser beam was focused into the water using an antireflection-coated lens with focal length of 100 mm. Between the laser and the focusing lens, the beam

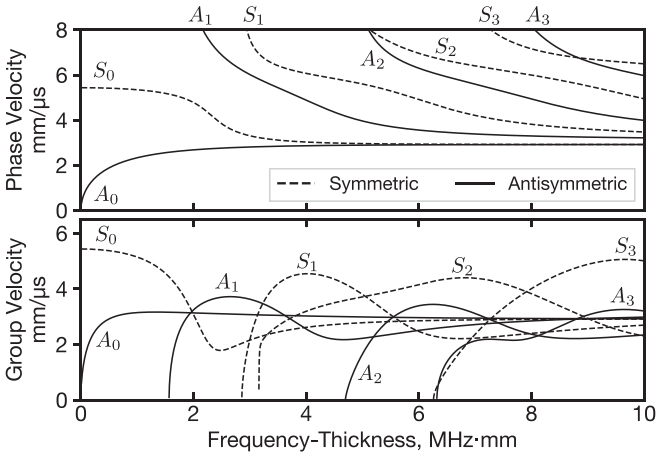

FIG. 2. Phase velocity (top) and group velocity (bottom) dispersion curves for Lamb waves, calculated numerically. The first four symmetric (dashed) and antisymmetric (solid) modes are plotted as a function of frequency-thickness product.

TABLE I. Sensing geometry for each measurement, as calculated using the travel time analysis described in the Appendix. d is the plate thickness, z_s is the source height from the plate, z_r is the receiver height, and r_0 is the initial receiver range for array measurements. In all experiments, the angular misalignment between the array and the plate was negligible ($|\theta| < 0.3°$).

d [mm]	z_s [mm]	z_r [mm]	r_0 [mm]
3.12	59.5 ± 0.8	126.2 ± 1.3	242.1 ± 1.0
6.45	76.9 ± 4.6	96.5 ± 5.4	257.5 ± 1.3
9.65	75.5 ± 5.2	92.6 ± 6.0	258.1 ± 1.3

energy was attenuated using a half wave plate and a polarizing beam splitter. The optical energy was monitored per-pulse by partially reflecting the attenuated beam to an energy meter.[15] Finally, the beam was redirected to the lens and focused into the water through the tank side-wall, which provided a consistent optical coupling interface. Accounting for losses along the beam path, the laser energy at the focus was typically 9.8 ± 0.2 mJ (peak optical power 1.5 MW).

The acoustic response of the system was measured using a 1 mm needle hydrophone with 20 MHz bandwidth (Onda HNR1000 with AH-1100 preamplifier). The hydrophone output was recorded using a USB oscilloscope with 25 MHz bandwidth and 8-bit ADC resolution. Hydrophone measurements were synchronized with the laser using the Q-switch output as a trigger, so that breakdown occurred at time $t = 0$. Array measurements were made by scanning the hydrophone parallel to the plate in 0.5 mm increments, over an array length of 60 mm. At each position, the plate response was averaged over 50 identical measurements in order to reduce noise and mitigate shot-to-shot variations in the acoustic source. Linear stage motion, laser firings, and hydrophone recordings were coordinated by a computer running custom software written in Python.

The source-plate-receiver sensing geometries were calculated using the travel time analysis described in the Appendix and are reported in Table I.

B. Sensing model

When a plate is insonified by a point source in the water, a hydrophone in the water will measure the superposition of three distinct signals corresponding to the three ray paths shown in Fig. 3(a). (1) A direct signal will propagate from the source to the receiver in the water, at a speed c_w. (2) The source excitation will specularly reflect off of the plate and the corresponding signal will arrive at the receiver a short time after the direct arrival. (3) The source will excite elastic waves within the plate, which travel laterally as guided modes (Lamb modes). As the guided modes propagate in the plate, the associated motion of the plate surface will reradiate energy into the fluid as acoustic plane waves.

In order to differentiate signals that travel in the water and in the plate, the arrival time of the signals can be used. Following Fig. 3(a), let r be the source–receiver range, z_s the source height, and z_r the receiver height. Using the length of the waterborne rays and the sound speed in water c_w, the arrival time of the direct (T_d) and reflected (T_r) signals are given by

$$T_d = c_w^{-1}\sqrt{(z_s - z_r)^2 + r^2}, \tag{1}$$

$$T_r = c_w^{-1}\sqrt{(z_s + z_r)^2 + r^2}. \tag{2}$$

To calculate the arrival time of a plateborne signal, its path must be traced through both the water and the plate. Acoustic energy can only be coupled between the water and a guided mode when the coincidence condition is satisfied: for a mode m at a frequency f, only a ray incident at $\theta = \theta_{c,m}(f)$ will couple to the mode. In the water the signal will propagate at c_w, while in the plate it will travel laterally at the mode's group velocity u_m. Since the reradiated acoustic wave must also satisfy the coincidence condition, the signal will reradiate to the receiver at the critical angle $\theta_{c,m}$. Therefore, the signal will travel a distance $L = r - (z_s + z_r)/\tan\theta_{c,m}$ in the plate and $L_w = (z_s + z_r)/\sin\theta_{c,m}$ in the water.

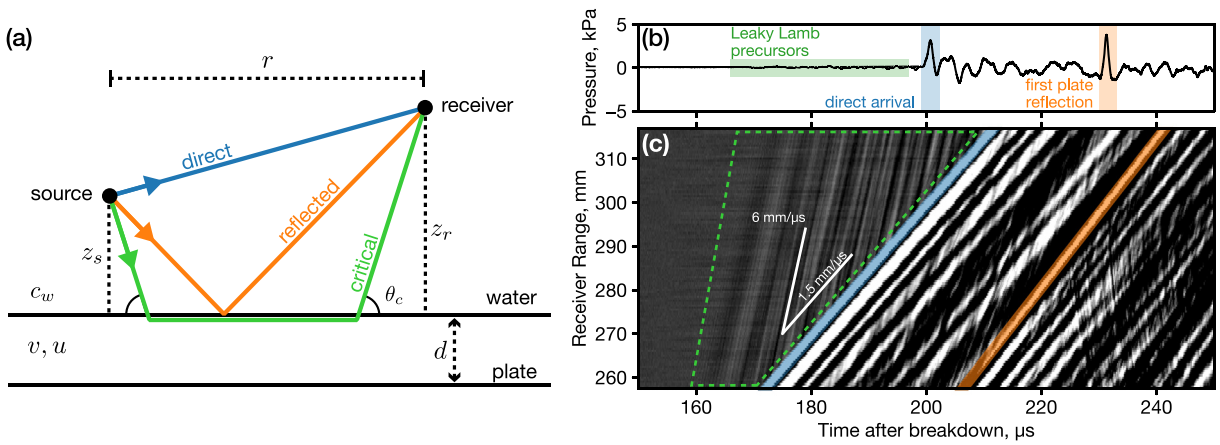

FIG. 3. (Color online) Sensing model and acoustic response of a $d = 6.45$-mm-thick plate to optical breakdown excitation. (a) A ray model predicts three signal paths between the source and receiver, including interactions with the plate: a direct path (blue), a specular reflection from the plate (orange), and a critical ray path that corresponds to leaky modes within the plate (green). (b) The pressure measured at a single hydrophone ($r = 300$ mm), can be interpreted in terms of the three arrivals predicted by the wave model. However, the arrivals along the critical ray path are very weak, and are not visible after the direct arrival because of a measurement artifact (large oscillations). (c) When measured with an array of receivers, the three signals propagate coherently along the array with distinct arrival time trajectories, as predicted by the ray model. For comparison, lines are drawn with slopes corresponding to 6 and 1.5 mm/μs. These predictions can be used to clearly identify and isolate the weaker Lamb mode signals (dashed green outline) for further analysis.

Noting that $\cos\theta_{c,m} = c_w/v_m$ and using trigonometric identities to substitute for $\tan\theta_{c,m}$ and $\sin\theta_{c,m}$, the total travel time for the critical ray can be expressed as

$$T_c = \frac{1}{u_m}\left(r - \frac{z_s + z_r}{\sqrt{v_m^2/c_w^2 - 1}}\right) + \frac{1}{c_w}\frac{z_s + z_r}{\sqrt{1 - c_w^2/v_m^2}}. \quad (3)$$

Because of the coincidence condition, the critical ray path is only defined for a source–receiver separation greater than $r_{\min} = |z_s + z_r|\,(v_m^2/c_w^2 - 1)^{-1/2}$,[16] which corresponds to the condition $T_c = T_r$. Therefore the receiver must be placed at a range $r > r_{min}$ to measure a leaky Lamb wave signal.

This model mostly mirrors the approach used to describe head waves in seismic modeling,[16] except here, dispersion is accounted for by explicitly separating the effects of fluid–elastic coupling (set by the phase velocity) from propagation within the plate (set by the group velocity).

For an array of receivers parallel to the plate (i.e., only r changing along array), Eqs. (1)–(3) reveal that the waterborne and plateborne signals will propagate along the array with different arrival time trajectories. Following the direct and reflected ray paths, the broadband source excitation will traverse the array with hyperbolic arrival times. Following the critical ray path, each leaky mode will radiate sound with an envelope that traverses the array with velocity $\partial T_c/\partial r = u_m(f)$. Within this envelope, coherent oscillations with frequency f will propagate at the phase velocity $v_m(f)$. The complete leaky Lamb wave signal will consist of coherent oscillations from modes at different m and f, which have spread out in time while propagating in the plate with different u_m.

This model has two important implications for sensing and analysis of leaky Lamb waves in the point-source/plate/array sensing geometry. First, hydrophone measurements of the plateborne signal will directly sample oscillations that travel with phase speed v_m. The remote measurements will thus sample the plate's dispersion spectrum and can be used to identify its mechanical properties. Second, the Lamb wave signals and the waterborne arrivals can be differentiated by their distinct travel time trajectories (linear vs hyperbolic). This travel-time difference also leads to a critical range r_c, beyond which the leaky guided modes out-pace the waterborne modes and arrive before the direct source signal. This occurs when $T_c \le T_d$, leading to a quadratic equation for r_c:

$$\left(\frac{u_m^2}{c_w^2} - 1\right) r_c^2 - \left(2\frac{z_s + z_r}{\sqrt{1 - \frac{c_w^2}{v_m^2}}}\frac{c_w^2 - u_m v_m}{c_w v_m}\right) r_c + \frac{u_m^2}{c_w^2}(z_r - z_s)^2 + \left(2\frac{z_s + z_r}{\sqrt{1 - \frac{c_w^2}{v_m^2}}}\right)^2 = 0. \quad (4)$$

Therefore, by spacing the source and receivers appropriately, it is possible to identify and isolate the leaky Lamb wave signals as precursors to the direct signal.

III. RESULTS

When the plates were insonified by the breakdown source, the hydrophone recorded a signal made up of three core components as described in the sensing model. The response is shown for the 6.45-mm-thick plate in Fig. 3(b), with the three signal components highlighted. The direct and reflected signals were sharply peaked, reflecting the loud, broadband source excitation. The leaky Lamb wave signal, by contrast, was 10–20 times weaker, and consisted of an oscillating, dispersive signal that is barely visible in Fig. 3(b). An additional oscillating signal was observed following the direct and reflected peaks for each hydrophone position. These oscillations were most likely measurement artifacts arising from the frequency-dependent receiver directivity and the oblique incidence of the broadband source pulse onto the hydrophone.

Because the leaky Lamb wave responses were so weak compared to the other signals, it was necessary to isolate them by placing the receiver array at a range $r > r_c$ from the source. Then, the Lamb wave signals arrived as precursors to the direct signal and could clearly be identified by their linear propagation along the array. As shown in Fig. 3(c), the Lamb wave signal travels across the array with a lateral phase velocity around 6 mm/μs. For comparison, the direct and reflected signals arrive along the array with hyperbolic travel times, asymptotically approaching the speed of sound in water, $c_w = 1.5$ mm/μs.

To analyze the frequency-domain structure of the plateborne modes, the Lamb wave signals were isolated using a time-domain mask that only kept signals arriving before the direct peak at $t = T_d$. Then, two different frequency transforms were used to characterize the plates' dispersive responses. First, a two dimensional fast Fourier transform (2 D FFT) was used to convert the masked hydrophone measurements (r-t domain) into the frequency-wavenumber (f-k) domain (Fig. 4), as has been used previously.[5,17] Second, a frequency-domain linear Radon transform was used to convert r-t data into the (phase velocity)-frequency (v-f) domain (Fig. 5). Conceptually, the amplitude of the v-f transform reflects the strength of a narrow-band wave packet, with center frequency f, traveling across the array at a phase velocity v. This transform can be realized as a linear Radon transform into the τ-v domain, followed by a 1 D FFT along the τ axis.[18,19] For both frequency transforms, the amplitudes were normalized by the source's spectral amplitude so that the plots reflect the strength of the radiating plate modes.

In the f-k domain (Fig. 4) the plate responses consisted of discrete peaks, corresponding to the discrete modes excited within the plates. The modal response extended across a wide-band window in both frequency ($f < 5$ MHz) and wavenumber ($k < 0.8$ mm^{-1}). Within this frequency window, the mode density increased with plate thickness, consistent with the expectation for guided modes.[2] As the frequency increases, the excited modes appeared along lines with slopes $f/k = 6.32$ and 3.13 mm/μs, which correspond to the elastic wave speeds in aluminum, c_L and c_T, respectively. Between these lines, minimal mode signatures could be observed.

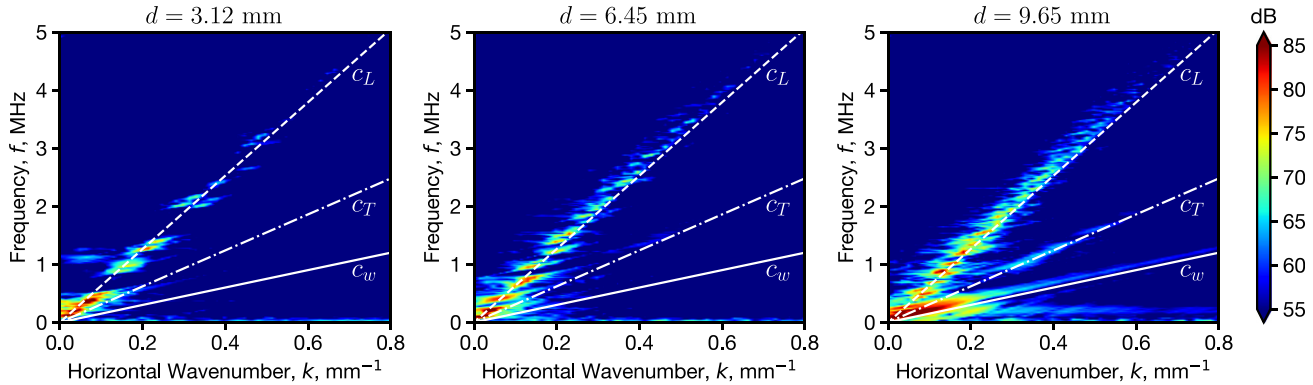

FIG. 4. (Color online) f-k spectra of leaky guided modes in three aluminum plates of different thickness. The log-magnitude spectrum is shown, normalized by the source's amplitude spectrum. The color bar applies to all three plots. For all plate thicknesses, discrete modes can be observed spanning frequencies up to 5 MHz. As the plate thickness increases from 3.12 mm (left) to 9.65 mm (right), more modes appear with higher density. For all plates, the strongest response is observed along a line where the phase speed is equal to the compressional speed ($v = f/k = c_L$). The white lines drawn on the plots correspond to the aluminum's compressional wave speed c_L (dashed), shear wave speed c_T (dashed-dotted), and the water's sound speed c_w (solid).

In the v-f domain (Fig. 5), the modal responses were more clearly separated, and the measured peaks overlapped well with the Rayleigh–Lamb dispersion curves for aluminum. Strong responses were observed from both symmetric and antisymmetric modes, S_n and A_n, respectively, for multiple orders n. The S_0 mode produced the strongest response for all plates, with higher-order modes producing progressively weaker responses. For the thinnest plate ($d = 3.12$ mm), the modes were widely spaced along the f-axis and distinct peaks could be clearly attributed to the S_0, A_1, S_1, A_2, S_2, and S_3 modes. As the plate thickness increased, additional modes could be observed at higher frequencies (e.g., 2.5 and 3.0 MHz for $d = 6.45$ mm plate), but the overlap of the higher-order dispersion curves made it difficult to attribute those responses to a specific mode. In all three plates, the excited modes appeared primarily in regions with phase velocity around the compressional speed in aluminum c_L, as was observed in the f-k domain.

In both frequency domains, the received modal peaks were consistently >20 dB higher than the background noise levels (decaying at higher frequencies). The mode amplitudes were clipped for plotting, but peaked at values as high as 90–100 dB.

IV. DISCUSSION

The frequency-domain results clearly demonstrate that a broadband leaky Lamb wave response can be excited by the breakdown source, and received with a waterborne receiver. The source's high spatial and temporal bandwidths make it possible to simultaneously excite multiple distinct modes within a broad f-k window, in contrast to the single mode coupling approach that has traditionally been used in immersion measurements.[7–9] However, the structure of the responses in Figs. 4 and 5 reveal that our measurements did not couple equally to all modes, or evenly across the observable range of frequencies and wavenumbers. Below we discuss how this restricted mode coupling can be explained primarily as a constraint imposed by the sensing geometry and signal processing used above. Then we discuss how these results can guide new non-contact guided-wave sensing strategies.

A. Leaky wave coupling

Our data contrast with previous observations of leaky Lamb waves in two ways. First, we observed responses primarily along a line of constant phase velocity $v \approx c_L$. Second, we observed stronger responses from symmetric modes than antisymmetric modes, even though antisymmetric modes are predicted to radiate more strongly because of their larger out-of-plane motion.[1–4] These differences in the leaky wave coupling can be explained by considering three factors specific to our sensing system: (1) the signal processing, (2) the sensing geometry, and (3) guided mode attenuation within the plate.

As described in Sec. II, the source and receiver were spaced far enough apart for plateborne signals to arrive as precursors to the direct waterborne signal. This structure allowed the plateborne signals to be isolated from the later signals and artifacts using a mask in the r-t domain. The r-t mask only sampled leaky Lamb modes with arrival times,

$$T_c(r) < T_d(r), \tag{5}$$

as shown in Fig. 3. Substituting Eqs. (1) and (3) into Eq. (5), the masking condition can be rewritten to identify which modes could be sampled by the receiver:

$$u_m > c_w \left(r - \frac{z_s + z_r}{\sqrt{v_m^2/c_w^2 - 1}} \right) \times \left(\sqrt{(z_s - z_r)^2 + r^2} - \frac{z_s + z_r}{\sqrt{1 - c_w^2/v_m^2}} \right)^{-1}. \tag{6}$$

Because of the masking, modes could only be observed at frequencies where the group velocity exceeds a threshold that depends on both the sensing geometry and the mode's phase velocity. Using the known values for the sensing geometry (from Table I), as well as $u_m(f)$ and $v_m(f)$ (from dispersion calculations), Eq. (6) predicts a measurable response in regions around $v_m \approx c_L$ and c_T, as indicated by the bright white segments of the dispersion curves in Fig. 5. These predictions overlap well with the measured response, indicating

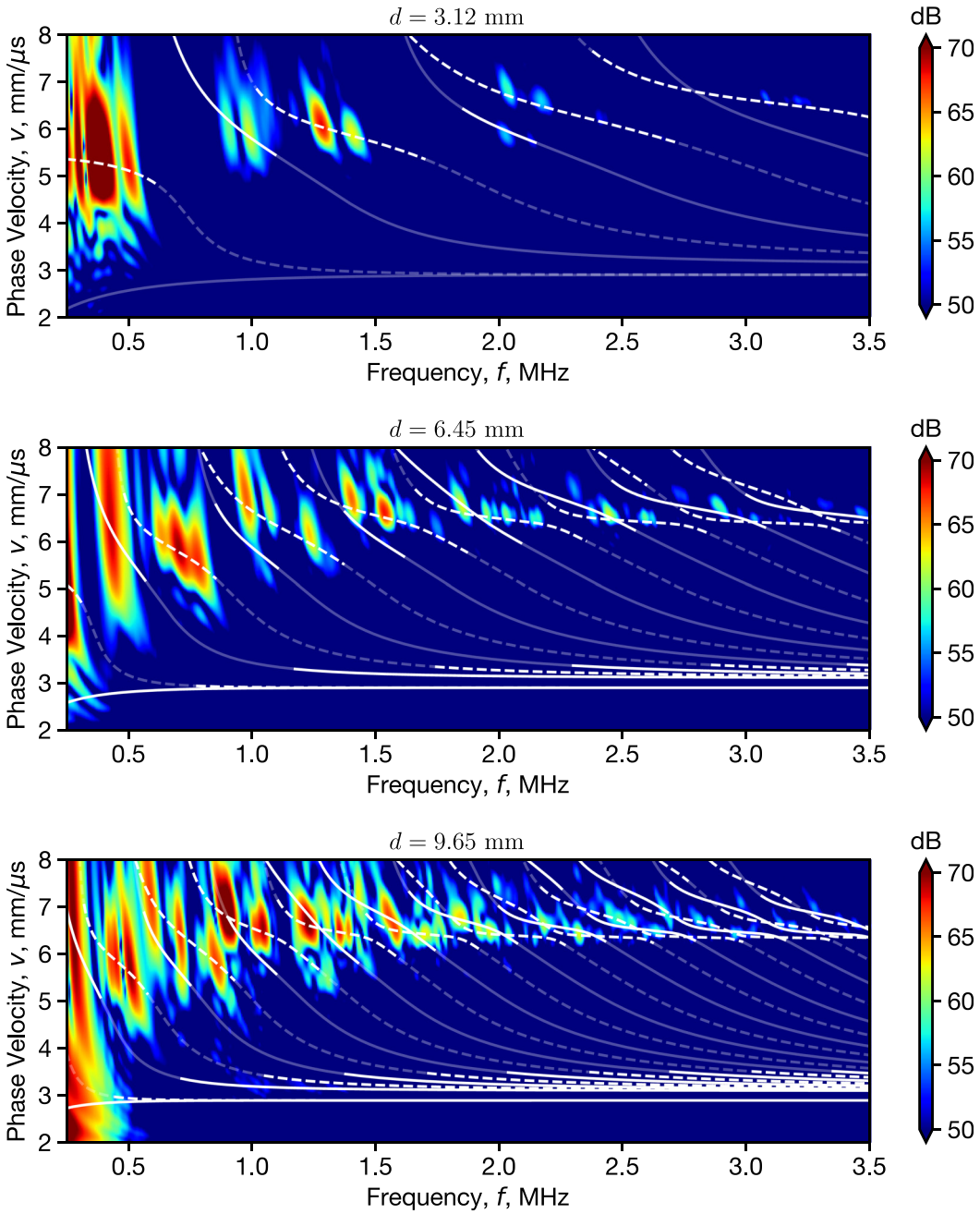

FIG. 5. (Color online) Phase velocity spectra for three aluminum plates of different thickness d. The log-magnitude spectrum is shown, normalized by the source's amplitude spectrum. The guided mode responses overlap with the predicted Lamb wave dispersion curves for each plate (white curves). The full dispersion curves are drawn faintly, while the predicted excitation from each mode is drawn brightly, based on Eq. (6). Responses arose from both symmetric modes (dashed curves) and antisymmetric modes (solid) for all plates. The lowest-frequency modes consistently produced the strongest response, and the mode amplitudes decayed with increasing frequency.

that the sensing geometry and masking governed the measurable response, to leading order.

While Eq. (6) reveals where leaky modes can be observed given the masking, this analysis does not predict the strength of the response within each observable region. For example, in the $d = 6.45$ and 9.65 mm plates, strong responses are expected around $v = c_T = 3.13$ mm/μs, but no signal was observable above the noise. Such amplitude predictions would need to account for the frequency-dependent radiation strength of each mode, which has been calculated previously by Bernard *et al.*[6] based on the complex wavenumber poles $k_m(f) + i\kappa_m(f)$ of the Green's function for the submerged plate. Whereas k_m represents the spatial wavenumber of a mode m at frequency f, κ_m represents the mode's attenuation as it propagates along the plate. Modes with high attenuation couple more strongly into the water, but also decay more rapidly as they propagate, making them only accessible to measurements at small ranges. Therefore, the measurement range will also limit which modes can be measured based on their attenuation. Comparing the results from Fig. 5 to the data from Bernard *et al.*, we observe responses from regions where the attenuation is relatively low, but non-zero. This effect is pronounced for the symmetric modes near $v = c_L$, where the attenuation goes to zero.[2,6]

By contrast, at their peak attenuation, the leaky Lamb modes decay at rates around $\kappa_m \approx 0.35$ dB/mm (scaled for 5 mm aluminum plate),[6] meaning the radiated signal would be 70 dB weaker after 200 mm propagating within the plate. Thus, compared to weakly attenuating modes, segments of the Lamb modes with high attenuation would not be strong enough to be observed in the present measurements.

This analysis indicates that the mode coupling in our experiments was set by the sensing geometry and signal processing in two ways. First, because of the time-domain mask, only modes with sufficiently high group velocity were received by the array and processed. Second, the attenuation of the guided modes set the radiating amplitude, but also how much energy could be propagated along the plate for long-range measurements. Given the long-baseline measurements above, strongly attenuating modes radiated too soon and only weakly attenuating modes could be observed by the receiver at large ranges.

Changes to the measurement geometry and signal processing would therefore make more modes accessible for non-contact measurement using this technique. Measurements at shorter range would better sample the strongly radiating modes, while measurements at larger ranges would collect stronger signals from low-group-velocity modes. Ongoing experiments with larger plates and larger source–receiver separations reveal responses from slower modes with phase velocities $v \approx c_T$.

A limitation imposed by our measurements was the masking of signals with $t < T_d$. In principle this mask is not necessary—the leaky Lamb signals persist beyond T_d and could provide access to more spectral information if they were included. However, in the measurements above, these late-arriving signals were overpowered by the acquisition artifact from the receiver's directionality. As a result, using the later arrivals in the signal processing only added more noise to the frequency spectra. If an omnidirectional receiver were used in this sensing configuration instead, the artifact would not be present and the late arrivals could be used to collect more information about the radiating modes. Then, by increasing the sampling window duration, signals from more modes could be collected without increasing the array length.

B. Optical breakdown guided wave sensing

These results suggest different sensing strategies that are possible with an optical breakdown acoustic source. By exciting and measuring a broadband response in the plate, the phase velocity spectrum can be compared to analytical dispersion curves to gauge a plate's thickness and material composition, as was done in Fig. 5. For simpler measurements, the mode separation that occurs based on group velocity could be used to identify the elastic wave speeds in the plate. Since the precursor signals cluster in the frequency domain around lines of $v = c_L$ and c_T (as shown by the measurements and predictions in Fig. 5), these early arriving signals could be analyzed to remotely gauge a material's elastic wave speeds based on the locations of group velocity maxima. Alternatively, since individual guided modes can be distinguished over a range of frequencies and wavenumbers, the different modes can be used to simultaneously identify mechanical features at different length scales and depths within the plate. By scanning the source in space, or repeating measurements over time, such measurements of the fixed modes could provide spatially or temporally resolved information about changing mechanical properties in a structure of interest.

These results are most directly applicable to submerged elastic structures that are much stiffer and denser than the surrounding fluid. As a material's stiffness and wave speeds drop, fewer modes can satisfy the leaky wave condition $v_m > c_w$ necessary for remote measurements. Moreover, materials with acoustic impedances similar to water will likely transmit most of the incident energy, so that little energy will be available to couple into guided modes. For materials whose densities approach that of water, it is also known that the Lamb mode dispersion spectra can change significantly.[20] Therefore, additional work remains to identify how effectively the source can be used to measure properties in materials whose densities and elastic wave speeds approach those of water.

V. CONCLUSION

Traditionally, remote Lamb wave measurements of underwater structures have required coincidence-matched immersion techniques or laser-thermoacoustic techniques that create sound directly on an object's surface.[7–9] However, these techniques impose constraints that can make it difficult to evaluate a broadband structural response in certain sensing environments. A more flexible approach would be to use a consistent, broadband, water-based acoustic point source to excite leaky Lamb waves.

In this paper, we have demonstrated how optical breakdown can be used as such an acoustic source for sensing. The breakdown source was used to excite a broadband leaky Lamb response in aluminum plates, which was measured with a hydrophone in the water. This sensing system measured excited modes across a broadband window of frequency ($f < 5$ MHz) and wavenumber ($k < 0.8\,\text{mm}^{-1}$). Both symmetric and antisymmetric Lamb modes were observed in the leaky response, with the strongest responses appearing along lines corresponding to phase velocity $v \approx c_L$. The mode clustering arose from an interplay of the signal processing, sensing geometry, modal group velocities, and modal attenuation. These results provide new opportunities for non-contact sensing and mapping of mechanical properties in underwater structures.

ACKNOWLEDGMENTS

A.G.A. thanks H. Schmidt, and the WHOI Ocean Acoustics and Signals group for valuable discussions, as well as L. Meroueh, D. Duane, and O. Vìquez for thoughtful feedback on the manuscript. This research was supported by the Office of Naval Research through award No. N00014-18-1-2066.

APPENDIX: SENSING GEOMETRY INVERSION FROM TRAVEL TIMES

In experiments, the source–receiver–plate geometry may not be known exactly *a priori*. To fully describe the sensing geometry, it is necessary to calculate the parameters

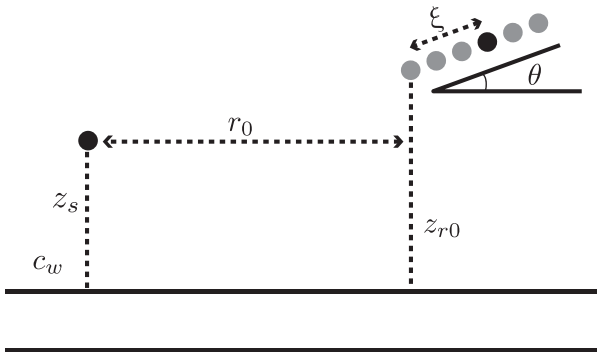

FIG. 6. Array geometry used to invert the sensing geometry from arrival time measurements. The geometry mirrors that in Fig. 3(a), but with a dip angle θ introduced to identify misalignment.

z_s, z_r, and r described in the text. Additionally, the array may not be exactly parallel with the plate, so the misalignment θ should also be identified ($\theta > 0$ corresponds to an array dipping away from the plate). This modified sensing geometry is shown in Fig. 6

These parameters can be calculated from measurements of the direct and reflected wave arrival times. If the spacing between receivers is known, then the position along the array can be described by the distance ξ. For any receiver along the array, the source–receiver range is given by $r = r_0 + \xi \cos\theta$, where r_0 is the range of the first receiver in the array. Similarly, the receiver height is given by $z_r = z_{r0} + \xi \sin\theta$, where z_{r0} is the height of the first receiver in the array. Substituting these values into the equations for T_d and T_r, the arrival times at any point along the array can be rewritten as quadratic equations in the known position along the array, ξ:

$$T_d^2 c_w^2 = \xi^2 + 2(r_0 \cos\theta - \Delta z \sin\theta)\xi + (r_0^2 + \bar{z}^2),$$
$$T_r^2 c_w^2 = \xi^2 + 2(r_0 \cos\theta + \bar{z} \sin\theta)\xi + (r_0^2 + 4\bar{z}^2),$$

where $\Delta z \equiv z_s - z_r$ and $\bar{z} \equiv (z_s + z_r)/2$ are defined to simplify notation. By measuring T_d and T_r at each position ξ along the array, the travel times can be fit to two parabolas—(T_d, T_r) vs ξ—with a least squares solver. The fit coefficients will then provide the sensing geometry (z_s, z_{r0}, r_0, θ). In the experiments described above, θ was negligible so that $z_r = z_{r0}$ for all receivers.

[1]I. A. Viktorov, *Rayleigh and Lamb Waves* (Plenum, New York, 1967), Chap. 2.
[2]J. L. Rose, *Ultrasonic Guided Waves in Solid Media* (Cambridge University Press, New York, 2014), Chap. 6.
[3]D. Hutchins, K. Lundgren, and S. Palmer, "A laser study of transient Lamb waves in thin materials," J. Acoust. Soc. Am. **85**, 1441–1448 (1989).
[4]D. Hutchins, D. Jansen, and C. Edwards, "Lamb-wave tomography using non-contact transduction," Ultrasonics **31**, 97–103 (1993).
[5]W. Gao, C. Glorieux, and J. Thoen, "Laser ultrasonic study of Lamb waves: Determination of the thickness and velocities of a thin plate," Int. J. Eng. Sci. **41**, 219–228 (2003).
[6]A. Bernard, M. Lowe, and M. Deschamps, "Guided waves energy velocity in absorbing and non-absorbing plates," J. Acoust. Soc. Am. **110**, 186–196 (2001).
[7]M. Karim, A. Mal, and Y. Bar-Cohen, "Inversion of leaky Lamb wave data by simplex algorithm," J. Acoust. Soc. Am. **88**, 482–491 (1990).
[8]M. Castaings and P. Cawley, "The generation, propagation, and detection of Lamb waves in plates using air-coupled ultrasonic transducers," J. Acoust. Soc. Am. **100**, 3070–3077 (1996).
[9]P. Rizzo, J.-G. Han, and X.-L. Ni, "Structural health monitoring of immersed structures by means of guided ultrasonic waves," J. Intell. Mater. Syst. Struct. **21**, 1397–1407 (2010).
[10]P. K. Kennedy, D. X. Hammer, and B. A. Rockwell, "Laser-induced breakdown in aqueous media," Prog. Quantum Electron. **21**, 155–248 (1997).
[11]A. Vogel, S. Busch, and U. Parlitz, "Shock wave emission and cavitation bubble generation by picosecond and nanosecond optical breakdown in water," J. Acoust. Soc. Am. **100**, 148–165 (1996).
[12]J. Noack, D. X. Hammer, G. D. Noojin, B. A. Rockwell, and A. Vogel, "Influence of pulse duration on mechanical effects after laser-induced breakdown in water," J. Appl. Phys. **83**, 7488–7495 (1998).
[13]S. V. Egerev, "In search of a noncontact underwater acoustic source," Acoust. Phys. **49**, 51–61 (2003).
[14]L. Mordfin, *Handbook of Reference Data for NonDestructive Testing (ASTM DS68-EB)* (ASTM, West Conshohocken, PA, 2002), Chap. 2.
[15]In separate experiments, the energy meter measurements were calibrated to the energy entering the water tank.
[16]K. Aki and P. G. Richards, *Quantitative Seismology*, 2nd ed. (University Science Books, Sausalito, CA, 2002), Chap. 6.
[17]P. Hora and O. Červená, "Determination of Lamb wave dispersion curves by means of Fourier transform," Appl. Comput. Mech. **6**, 5–16 (2012).
[18]O. Yilmaz, *Seismic Data Analysis*, 2nd ed. (Society of Exploration Geophysicists, Tulsa, OK, 2001), Chap. 6.
[19]R. Schultz and Y. Gu, "Flexible, inversion-based Matlab implementation of the Radon transform," Comput. Geosci. **52**, 437–442 (2013).
[20]S. Rokhlin, D. Chimenti, and A. Nayfeh, "On the topology of the complex wave spectrum in a fluid-coupled elastic layer," J. Acoust. Soc. Am. **85**, 1074–1080 (1989).